Polskie Towarzystwo Materiałów Kompozytowych
Polish Society of Composite Materials

25: 4 (2025) 226–233

COMPOSITES THEORY AND PRACTICE

ISSN (online): 2299-128X

Jagadish Chandra Padhi, Satyanarayan Bhuyan, Seshadev Sahoo*

Faculty of Engineering and Technology, Siksha 'O' Anusandhan Deemed to be University, Bhubaneswar 751030, India
* *Correspondence:* seshadevsahoo@soa.ac.in

Received (Otrzymano) 23.08.2025
Published on-line (Opublikowano) 31.12.2025

STRUCTURAL, MORPHOLOGICAL-TOPOLOGICAL, DIELECTRIC PROPERTIES OF BINARY METAL OXIDE Ni_2O_3-CO_3O_4 ELECTRONIC MATERIAL

https://doi.org/10.62753/ctp.2025.01.4.4

The distinctive solid state mixed oxide-based step-sintering technique was used to fabricate nickel cobaltite ($NiCo_2O_4$) material from Ni_2O_3 and Co_3O_4. The material's attributes, namely crystallite size of 40.06 nm with minimal strain of 0.0024, dislocation density 8.4×10^{14} m^{-2} and cubic crystal structure were revealed by means of X-ray diffraction and the W-H method. SEM micrographs of the microstructure reveal polycrystalline grains of different sizes with clear grain boundaries and an evenly aligned grain texture. This material has been proven to be a suitable capacitive component for advanced electronic applications with the aid of experimentally investigated structural features, grain distribution topography, polar histogram and temperature dependent frequency dispersion dielectric spectra. This material is a desirable candidate for device designs since it exhibits relatively high dielectric permittivity and low dielectric loss at high frequencies, indicating minimum energy dissipation. The results and analysis affirm the dielectric properties, lending credence to the idea that nickel cobaltite could be a viable oxide-based ceramic entity for appropriate device applications.

Keywords: ceramic mixed oxides, $NiCo_2O_4$ material, topology, dielectric response

INTRODUCTION

Oxide-based ceramic materials are preferential over other materials in the fields of industrial and research applications because of their remarkable qualities, such as physico-chemical stability and thermal-electrical-mechanical resistance [1–3]. The demand for these materials is currently rising globally in environmental, biomedical and electronics engineering due to their numerous applications as sensors, catalysts and energy storage devices [4–8]. Among different oxides, the mixed-valence oxide has been preferred for electronic device design because of its superior electrochemical qualities, advantageous pseudo-capacitive actions (high specific capacitance with the ability to store a considerable amount of charge), interesting cycle stability (multiple instances of charging followed by discharge), and favourable electrical conductivity. Particularly, the combination of nickel (III) oxide (Ni_2O_3) and tricobalt tetraoxide (Co_3O_4) based mixed-valence oxide ceramic material is becoming increasingly more popular as a dielectric material for high-performance energy storage, catalysis and capacitive sensing [9–11]. The inexpensive cost of Ni_2O_3, relatively simple structure, high band gap (~3.52ev) at ambient temperature, and superior theoretical capacity

have made it a promising entity for electronic device applications [12]. Other material dielectric characteristics can be altered by using Ni_2O_3, which is known to have a comparatively high dielectric constant. Conversely, the existence of oxygen vacancy can affect the properties of Ni_2O_3 based ceramic devices, which may result low responsiveness and disrupt the linearity. To increase the effectiveness and performance of Ni_2O_3 oxide ceramics, doping and/or mixed-oxide techniques are therefore frequently employed [13]. The performance of the material can be improved by combining with other materials owing to its improved conductivity and capability to buffer volume changes. In this regard, tricobalt tetraoxide (Co_3O_4) ceramics are often combined with Ni_2O_3 due to its accessibility, affordability, as well as exceptional thermal and chemical stability [14]. The Co_3O_4 ceramic is a semiconducting antiferromagnetic material whose lattice contains cobalt cations Co^{2+} and Co^{3+} ions that are dispersed in tetrahedral and octahedral interstitial spaces with a characteristic spinel structure. The oxygen vacancies and structural deformation brought on by Co_3O_4 ceramic material mainly change the device's performance and its ability to remain nearly temperature stable across a broad temperature range.

Considering the outlined facts, in the present investigation nickel cobaltite electronic ceramic material with the compositional formula $NiCo_2O_4$ was processed from Ni_2O_3 and Co_3O_4 as initial materials with the help of an innovative solid state mixed-oxide based step-sintering technique. To prepare nickel cobaltite using different precursor materials, researchers have to date employed a variety of synthesis methods [15–16], including solvothermal synthesis, hydro-thermal jet fusion, the sol-gel technique, co-precipitation and thermal decomposition. To our knowledge, no other research group has published a paper on nickel cobaltite synthesis using a low temperature solid state mixed-oxide based step-sintering synthesis process, which is versatile, sustainable and easy to carry out in comparison to other reported synthesis methods. The advantages of this synthesis technique over conventional methods of processing include its rapid heating rate with step-sintering, a suitable isothermal retaining technique, in addition to a considerably reduced temperature and processing time. The growth of crystalline phases, morphology, visible grains with boundaries that lead to space charge polarization are aided by this synthesis process. An experimental investigation and comprehensive analysis were carried out in order to reveal the ceramic's structure formulation, morphology and grain distribution, as well as dielectric response that is dependent on temperature and frequency.

MATERIAL SELECTION AND PREPARATION OF SPECIMENS FOR INVESTIGATIONS

Utilizing analytical quality (>99.9% pure) powders of nickel (III) oxide (Ni_2O_3) and cobalt (II, III) oxide (Co_3O_4) as starting materials supplied by Loba Chemicals Pvt. Ltd., India, the ceramic $NiCo_2O_4$ was created utilizing a traditional solid state reaction procedure. To produce a uniform blend of these two unprocessed oxides, a 34:66 molecular weight percentage ratio of the powders was extensively dry milled for around five hours. After adding 75 millilitres of 70% pure methanol, the mixture was wet ground until the methanol slowly evaporated. This resulted in a fine powder, which was subsequently kept in an alumina crucible and calcined in a muffle furnace at 660°C for four hours. Fig. 1 shows the fabrication process. The process follows the basic chemical reaction described below.

$$\frac{1}{2}Ni_2O_3 + \frac{2}{3}Co_3O_4 \rightarrow NiCo_2O_4 + \frac{1}{12}O_2 \uparrow \qquad (1)$$

Following completion of the calcination process, the material was reground for structural examination and X-ray diffraction (XRD) analysis to determine the composition of the ceramic. Using an optical wavelength of 1.5405 Å and a searching pace of 2°/min, XRD analysis was performed within the Bragg angle $20° < 2\theta < 80°$ range. Then the composition was mixed with PVA (polyvinyl alcohol) to make discs (10 mm × 2 mm) by

applying a compact pressure. The resulting discs were sintered for four hours at 660°C on an alumina boat. The surface morphology was investigated by means of SEM to examine the surface topology for structure-property relations. An analytical grade silver paste was used as electrodes on both of the disc surfaces in order to perform different electrical experiments (using a ZM-2376 LCR meter from the NF Corporation). Parameters such as dielectric loss, relative permittivity, conductivity and impedance were evaluated at 1–1000 KHz (frequency range) and 35–400°C (temperature range).

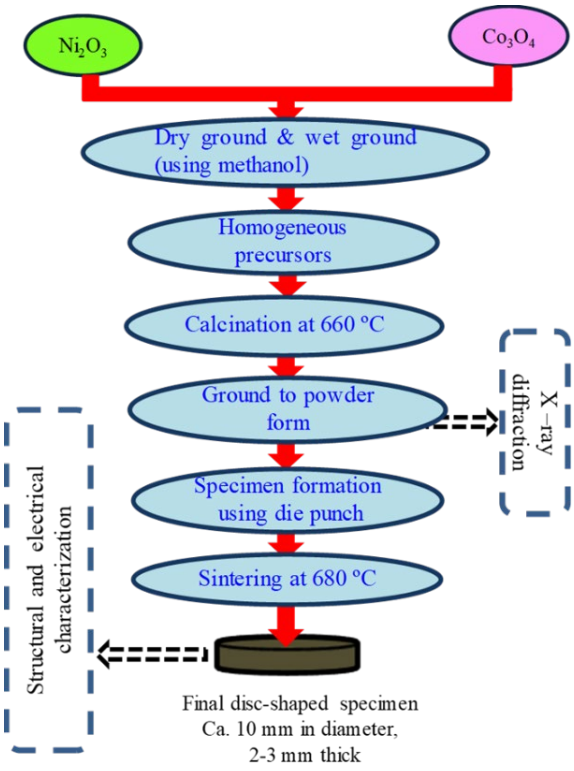

Fig. 1. $NiCo_2O_4$ specimen production process

COMPREHENSIVE ANALYSIS AND DISCUSSION OF RESULTS

Structural features

The XRD pattern of the $NiCo_2O_4$ sinter is presented in Fig. 2. The polycrystalline nature was verified by indexing the Miller indices of clear-sharp peaks with the help of X'Pert High Score software.

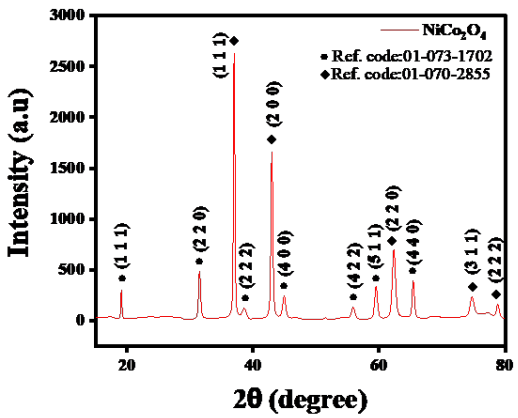

Fig. 2. X-ray diffraction pattern $NiCo_2O_4$

The XRD peaks were indexed according to cubic $NiCo_2O_4$ (JCPDS file # 01-073-1702) and cubic CoO (JCPDS file # 01-070-2855) ceramics. The Debye-Scherrer formula was used to calculate the crystallite size, $C_s = G\lambda/\beta\cos\theta$ and dislocation density $\delta = 1/(C_s)^2$. C_s = geometrical factor = 0.9, λ = 1.5405 Å = X-ray wavelength, θ = diffraction Bragg angle, β = FWHM: full width at half maximum (in radians) [17]. The assessed crystallite size and dislocation density were found to be 34.5 nm and 8.4 × 1014 m-2 respectively.

Williamson-Hall (W-H) method

The W-H method, which successfully finds the material's microstrain and typical crystallite size by examining the slope and intercept of the $\beta\cos\theta$ vs $4\sin\theta$ plot, is depicted in Fig. 3. In the figure, the FWHM of the diffraction peaks is plotted against the scattering vector or angle on a graph. The W-H method finds the broadening of diffraction peaks by simultaneously considering the strain effects as well as the size [17]. The impact of defects and dislocations on the strain within the crystal lattice is taken into account. The overall widening is determined by the cumulative effects of crystallite size and strain, expressed as $\beta_{Cs} = \beta_D + \beta_{\epsilon s}$, where β_{Cs} represents the overall broadening, β_D indicates the broadening attributed to the size effects of crystallites ($\beta_D = G\lambda/C_s\cos\theta$), and $\beta_{\epsilon s}$ is the strain-induced broadening, ($\beta_{\epsilon s} = 4\epsilon\tan\theta$) the peak owing to microstrain, the observed peak position in radians is denoted by θ, while ε represents the developed strain.

Comparing the equation of the straight line $y = 0.004 + 0.0024\,x$ given in Fig. 2 with the Williamson-Hall relation $\beta_{Cs}Cos\theta = (G\lambda/C_s) + 4\epsilon sin\theta$, the crystallite size of the $NiCo_2O_4$ sample is calculated to be 40.06 nm and the strain is equal to slope 'ε', i.e. 0.0024, while the y-intercept ($G\lambda/ C_s$) is 0.004. The main reason why the Debye-Scherrer formula crystallite size calculation is different from the Williamson-Hall method is that the former alone takes crystallite size into account, whilst the latter separates the effects of size and microstrain on peak broadening.

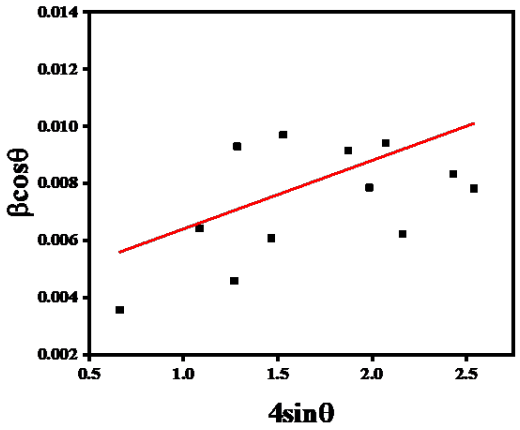

Fig. 3. W-H plot of $NiCo_2O_4$ ceramic

SEM morphology and topography analysis with histogram

The specimens were extensively sintered at the temperature of 680°C, which greater than the calcination temperature, to achieve a compact microstructure and avoid surface porosity. Fig. 4(a) shows scanning electron micrographs of the $NiCo_2O_4$ ceramic material. The micrograph of the specimen shows that the surface of the sinter is uniformly covered in minute grains of different shapes, with a few spots of unfilled volume here and there. The grains are polycrystalline, come in a range of sizes, and have well defined edges. There is a noticeable varied range in particle size as seen in the histogram of the particle size distribution made from the SEM micrograph of the same ceramic substance in Fig. 4(b). The average diameter of the particles is 5.14 μm, and their sizes range from 1 μm to 9 μm. The scanning electron micrograph of the ceramic shows a three-dimensional surface topography with a 95.15 mm peak-to-valley height range, as shown in Fig. 4(c). The variegation is indicative of a surface that is rather uneven and has visible grains, troughs, and ridges. The various surface heights represent inherent surface roughness and grain boundaries. The angular distribution, crystallographic orientation, or directional defects can be studied using the semi-circular rose plot. The blue lines in the plot shown in Fig. 4(d) represent the size or frequency of features aligned at angles between 0 and 180 degrees. The isotropy value of 33.50% indicates that the pattern is moderately isotropic. The surface stiffness and grain texture are clearly aligned due to the moderate isotropy value. Three primary directions 90°, 114°, and 128.8° correspond to the grain and structural alignments in the mixed ceramics. The polar histogram depicted in Fig. 4(e) shows the orientation and microstructure of the material grains and crystalline structure. In relation to the mean direction of all the orientations, the width of each bin reveals precise data orientation. A moderate degree of directional dependency is displayed by the structure, with its structural parts centred between 53.31° and 63.67°.

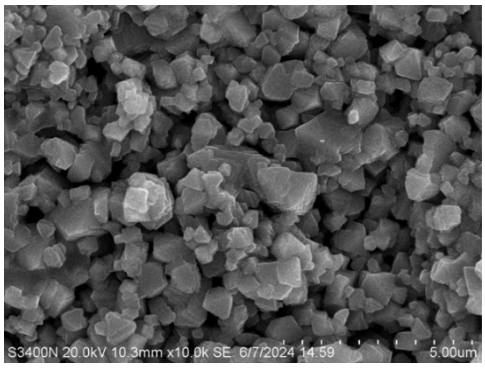

a)

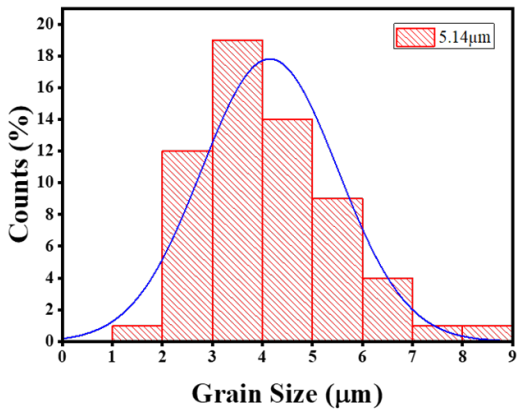

b)

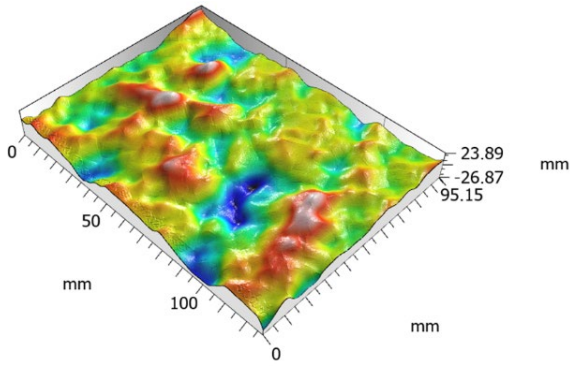

c)

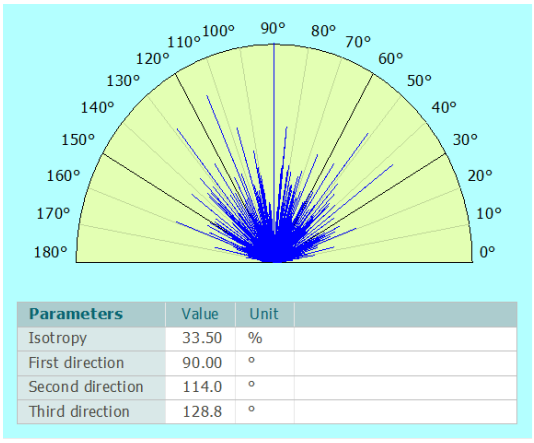

Parameters	Value	Unit
Isotropy	33.50	%
First direction	90.00	°
Second direction	114.0	°
Third direction	128.8	°

d)

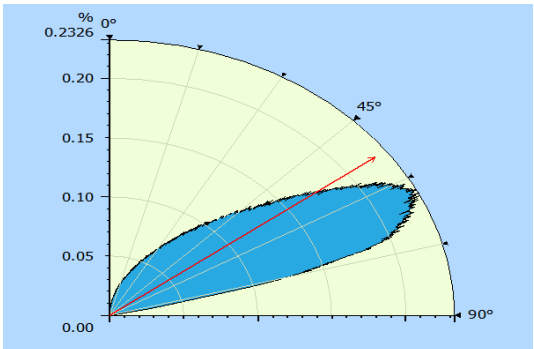

Information	
Angle	Polar angle (alpha)
Number of bins	1109
Width of each bin	0.081154 °

Parameters	Value	Unit
Circular mean	53.31	°
Mean resultant length	0.9606	
Main	63.67	°

e)

Fig. 4 (a) SEM micrograph, (b) particle size distribution histogram, (c) micrograph topography, (d) polar graph with isotropy, (e) polar histogram to represent grain orientation

Analysis of NiCo2O4 material temperature--frequency dependent dielectric property

By means of dielectric spectroscopy, the electrical and dielectric properties of the produced material were examined. This test method is useful for finding the dissipation factor and relative permittivity of the material across a wide frequency and temperature range. The distribution of the E-field inside the sample determines the dielectric characteristics of the material. The transport mechanisms and structural change of a material can be inferred from its dielectric constant and loss dependencies on frequency and temperature. The kind of defects, the amount and kind of polarization that relaxes the material, the origin of dielectric loss, and other related details can be determined by dielectric investigations. After measuring the dissipation factor and capacitance with the LCR instrumental setup, the permittivity and loss tangent can be calculated. The relative dielectric constant for the treated material can be determined by dividing the capacitance of the material by its permittivity, and then using the formula $\varepsilon r = C_p d/\varepsilon_0 A$, where the material capacitance is C_p, area A, thickness d, and permittivity ε_0. To determine the loss tangent (tan δ), one might utilize the dissipation factor. The relationship between temperature and relative permittivity (ε_r) at designated frequencies is illustrated in Fig. 5, while the loss tangent (tanδ) is presented in Fig. 6. The increase in the dielectric constant at low frequencies was found to be independent of temperature (i.e. up to 300°C) as a result of the existence of various types of polarizations within the material. The polarization effect diminishes progressively as the frequency increases, leading to a reduction in the dielectric constant. The ε_r curve exhibits a gradual increase with temperature, becoming notably sharp at 377°C, identified as the phase transition temperature, before it begins to decrease gradually. As the temperature rises, space charges migrate to the grain boundary area and accumulate, resulting in oxygen vacancies that contribute to an increase in the dielectric constant value [18].

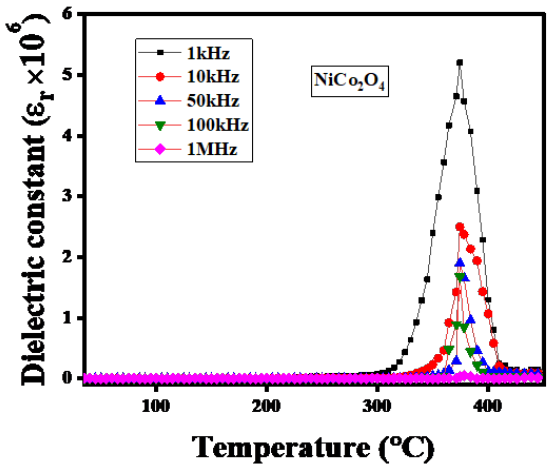

Fig. 5. Dielectric constant temperature dependency of $NiCo_2O_4$ at specific frequency

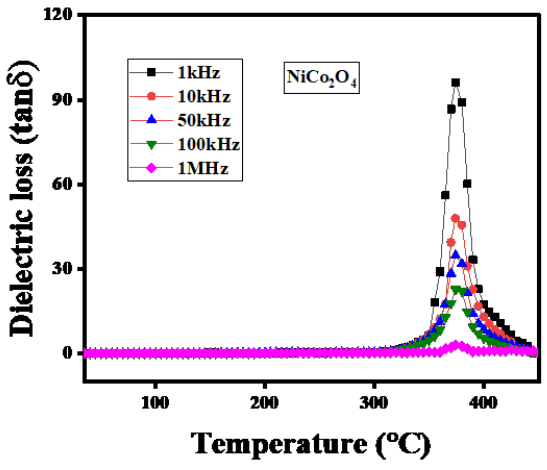

Fig. 6. Tangent loss temperature dependency of $NiCo_2O_4$ at specific frequency

Similar to the reported characteristics of ε_r, the tendency of the loss tangent (tanδ) to fluctuate with regard to temperature-frequency is also illustrated. At high temperatures, the loss tangent (tanδ) grows substantially, but at low temperatures, it grows less. The observed dielectric loss peaks are believed to be caused by thermally accelerated relaxation processes in the $NiCo_2O_4$ lattice, such as polaron hopping or defect dipole relaxation. Because charge carriers and dipoles have more time to align with the alternating field at lower frequencies, dielectric losses are greater at those frequencies. The loss decreases as the frequency increases due to the ability of dipoles to track the field. According to Arrhenius-type phenomenon, which asserts that higher frequencies require more thermal energy for polarization, the peak moves toward higher temperatures as the frequency increases. It may be a suitable option for applications involving high frequencies due to $NiCo_2O_4$'s reduced energy dissipation and its observed low dielectric loss at 1 MHz.

Figs. 7 and 8 show how the relative dielectric constant (ε_r) and loss tangent (tanδ) of the produced dielectric sample change with frequency over a temperature range of 35 to 400°C. A frequent feature of dielectric material is that both parameters drop as the frequency increases. In the low-frequency range, the material reveals a higher ε_r value, which may be due to electron accumulation caused by space charge polarization. One can see that tanδ grows quickly at low frequencies from the frequency-loss tangent spectrum, but its value drops sharply with increasing temperature. The particular dielectric behaviour of this ceramic can be explained by several polarization processes, including atomic, ionic, dipolar, and interfacial polarization, which can be studied using the Maxwell-Wagner effect and Koop's phenomenological theory [19]. High relative permittivity and dissipation factors are produced by a number of processes, including the build-up of space charges, the motion of electron clouds, the field-directed orientation of dipoles, and short-distance ion separation at low frequencies (100 Hz). Since only electrons are capable of perceiving the quick shift in frequency, the total polarization diminishes as the frequency is reduced, leading to the lowest values of ε_r and tanδ at high frequencies.

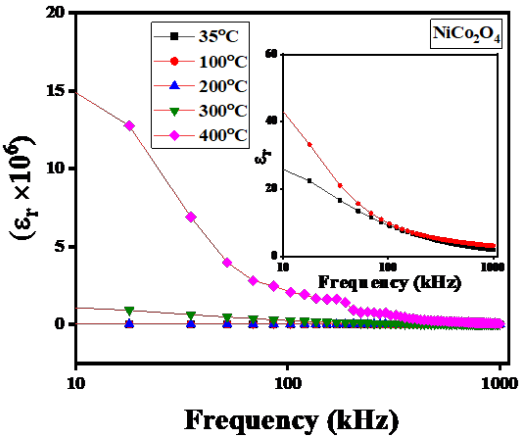

Fig. 7. Dielectric constant frequency dependency of $NiCo_2O_4$ at specific temperature

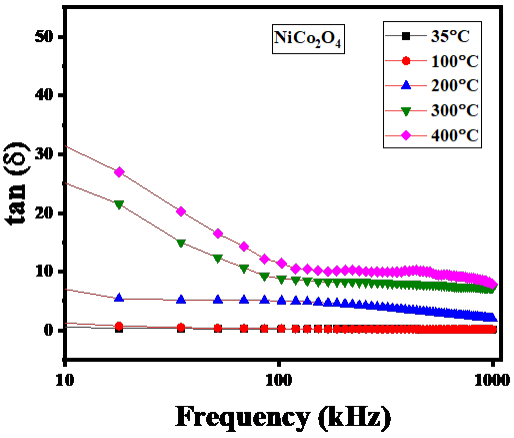

Fig. 8. Tangent loss frequency dependency of $NiCo_2O_4$ at specific temperature

CONCLUSIONS

The current study used a mixed-oxide low temperature solid state reaction-based approach to produce a new $NiCo_2O_4$ ceramic material. X-ray diffraction analysis clarified the material properties with regard to strain, crystallite size, and crystal structure. The crystallite size and microstrain of this material were successfully ascertained using the W-H approach. The low value of isotropy makes it clear that the grain texture and stiffness on the material surface are aligned uniformly. Thermally stimulated relaxation mechanisms, such as polaron hopping or defect dipole relaxation in the $NiCo_2O_4$ lattice, are thought to be responsible for the observed dielectric loss peaks. Owing to the experimentally investigated temperature-dependent electrical properties, this $NiCo_2O_4$ oxide based ceramic material has been proven to be a suitable capacitive component for a wide range of advanced electronic devices and industrial applications.

REFERENCES

[1] Raz Muhamma, Yaseen Iqbal, and Ian M. Reaney, Ba-TiO3–Bi (Mg2/3Nb1/3) O3 ceramics for high temperature capacitor applications, Journal of the American Ceramic Society, 99 (6) 2089-2095, 2016. https://doi.org/10.1111/jace.14212

[2] L. Sahoo, S. Bhuyan and S.N. Das, Tin oxide-titania based electronic system: synthesis, structural, microstructural and dielectric properties, 23: 4, 183-190, 2023. https://doi.org/10.62753/ctp.2023.01.4.4

[3] P.V.C.K. Subhashini, K.V.D. Rajesh, Comparative performance assessment of nano-composite cathode of LMSO-BSCMF for low temperature solid oxide fuel cell applications, 23: 4, 235-238, 2023. https://doi.org/10.62753/ctp.2023.08.4.4

[4] K.S. Randhawa, Advanced ceramics in energy storage applications: Batteries to hydrogen energy, J. Energy Storage 98, 113122, 2024. https://doi.org/10.1016/j.est.2024.113122

[5] Melvin M. Vopson, Fundamentals of multiferroic materials and their possible applications, Critical Reviews in Solid State and Materials Sciences, 40 (4), 223-250, 2015. http://dx.doi.org/10.1080/10408436.2014.992584

[6] M. Bhavisha, K. Anjali, S. Aswani, A. Sakthivel, Catalytic applications of perovskites, in Ceramic Catalysts, Elsevier, pp. 19–55, 2023. https://doi.org/10.1016/B978-0-323-85746-8.00005-9

[7] P. Harshapriya, D. Basandrai, P. Kaur, Structural, magnetic, microwave absorption and electromagnetic properties of Y-Ag-doped bismuth ferrite nanoparticles for commercial applications, Appl. Phys. A 129 (316), 2023. https://doi.org/10.1007/s00339-023-06535-y

[8] M. Rangi, S. Sanghi, S. Jangra, K. Kaswan, S. Khasa and A. Agarwal, Crystal structure transformation and improved dielectric and magnetic properties of La-substituted $BiFeO_3$ multiferroics, Ceramics International, 43 (15), 12095-12101, 2017. https://doi.org/10.1016/j.ceramint.2017.06.065

[9] J. Hwang, J.H Jin, H. Kim, K.Y. Lee, I.H. Yang, Fabrication of Ni_2O_3–NiCx core–shell nanoparticles on fluorine-doped tin oxide electrodes via oxygen feeding from SnO_2 under hydrogen conditions and their electrochemical performance as supercapacitors, Colloid and Interface Science Communications, 44, 100470, 2021. https://doi.org/10.1016/j.colcom.2021.100470

[10] S. Karmakar, S. Varma, D. Behera, Investigation of structural and electrical transport properties of nano-flower shaped $NiCo_2O_4$ supercapacitor electrode materials, Journal of Alloys and Compounds, 757, 49-59, 2018. https://doi.org/10.1016/j.jallcom.2018.05.056

[11] R. Ahmad, A. Sohail, U. Altaf, J. Farooq, A. Mir, M. Aalim, A. Majeed, M.A. Shah, Binary nickel cobalt oxide ($NixCo_3$-xO_4) nanostructures as stable and high-energy density asymmetric supercapacitor electrode material, Materials Chemistry and Physics, 307, 128195, 2023. https://doi.org/10.1016/j.matchemphys.2023.128195

[12] Jiayou Mou, Chenxi Wang, Run Pan, Guanlin Zhang, Shuai Liu, Honglei Zhang, Jing Wang, Yong Ren, A novel z-type heterojunctioned Ni_2O_3 composite catalyst for photocatalytic hydrogen generation, International Journal of Hydrogen Energy, Volume 154, 150295, 2025. https://doi.org/10.1016/j.ijhydene.2025.150295

[13] Fei Sun, H. Zhao, K. Miao, Influence mechanism of Ni_2O_3 doping on leakage current of SnO_2 varistor ceramics, 21(5), 3089-3096, 2024. https://doi.org/10.1111/ijac.14785

[14] X. Wang, W. Tian, T. Zhai, C. Zhi, Y. Bando and D. Golberg, Cobalt(II,III) oxide hollow structures: fabrication, properties and applications, J. Mater. Chem., 22, 23310-23326, 2022. https://doi.org/10.1039/C2JM33940D

[15] J. Marco, J. Gancedo, M. Gracia, J. Gautier, E. Rıos and F. Berry, Characterization of the Nickel Cobaltite, $NiCo_2O_4$, Prepared by Several Methods, An XRD, XANES, EXAFS, and XPS Study, J. Solid State Chem., 153, 74-81, 2000. 10.1006/jssc.2000.8749

[16] S. Chaudhari, D. Bhattacharjya and J.S. Yu, Facile Synthesis of Hexagonal $NiCo_2O_4$ Nano-plates as High-Performance Anode Material for Li-Ion Batteries. Bull. Korean Chem. Soc., 36, 2330–2336, 2015. https://doi.org/10.1002/bkcs.10462

[17] S. Kalingani, S.N. Das, S. Bhuyan, Structural, micro-structural, morphological, electrical spectroscopy and optical analysis of lithium–titanium oxide electronic material, Inorg. Chem. Commun. 159, 111731, 2024. https://doi.org/10.1016/j.inoche.2023.111731

[18] S. Halder, S. Bhuyan, R.N.P. Choudhary, Structural, dielectric and electrical properties of bismuth magnesium tantalate electronic system, J. Magn. Alloys 7(4), 628–636, 2019.https://doi.org/10.1016/j.jma.2019.07.008

[19] S.K. Samal, B. Biswal, M.K. Mallick, R.N.P. Choudhary and S. Bhuyan, Frequency-temperature-dependent electrical properties of fabricated (Pb0.7Bi0.15Sm0.15)(Ti0.7Fe0.3)O3 capacitive electronic material component, Appl. Phys. A 128, 683 (2022). https://doi.org/10.1007/s00339-022-05827-z